Applied Thermal Engineering 180 (2020) 115767

Contents lists available at ScienceDirect

Applied Thermal Engineering

journal homepage: www.elsevier.com/locate/apthermeng

Nozzle scaling effects for the thermohydraulic performance of microjet impingement cooling with distributed returns

T.-W. Wei[a,b,*], H. Oprins[a], Liang Fang[b], V. Cherman[a], I. De Wolf[c], E. Beyne[a], M. Baelmans[b]

[a] imec, Leuven, Belgium
[b] Dept. Mech. Eng., KU Leuven, Leuven, Belgium
[c] Dept. Materials Eng., KU Leuven, Leuven, Belgium

HIGHLIGHTS

- The impact of nozzle density for 3D printed jet cooler is experimentally measured.
- A numerical parameter sensitivity study is used to find optimal jet cooler design.
- Constant cooling rate/pumping power requires different optimal design parameters.
- Best design nozzle density is between 30 cm^{-2} and 300 cm^{-2} for constant flow rate.
- Best design with highest nozzle density is for constant pumping power comparison.

ARTICLE INFO

Keywords:
Impingement cooler
Additive manufacturing
Nozzle density
Numerical modeling
Cavity height
Coefficient of performance

ABSTRACT

Previous research studies showed that bare die liquid multi-jet impingement coolers with locally distributed outlets using silicon processing, mechanical micromachining, and additive manufacturing technology can achieve high cooling efficiency for high power electronic applications. The nozzle density is a crucial factor for thermal performance as well as for selecting the required fabrication technology. However, general design guidelines for the optimal nozzle density and cavity height are still missing in literature. In this paper, the impact of nozzle density on direct multi-jet impingement jet cooling is investigated using experiments and numerical modeling for an N×N nozzle array. The general scaling analysis with experimentally validated models is investigated based on three independent design parameters: nozzle density (N^2/A), nozzle diameter (d_i) and cavity height (H). The objective is to find the optimal design parameters and to study the scaling trends. The experimental studies show that a very good thermal performance for the 8 × 8 jet array cooler with 1 × 1 mm^2 cooling cells has be achieved as low as 0.13 cm^2-K/W for a flow rate of 1000 ml/min. The best cooler design, expressed as the cooler with the highest COP value, can be achieved in the middle range of the nozzle density between 30 and 300 nozzles per cm^2 for the constant flow rate consideration. Comparisons in terms of constant cooler flow rate or constant pumping power will result in different optimal design parameter values.

1. Introduction

Thermal management of high-power devices (MOSFETs, IGBTs) or high-performance systems (2.5D, 3D integration), is becoming more and more challenging. It is expected that the heat flux for future high-power devices is on the order of 600–1000 W/cm^2 [1]. Therefore, advanced cooling concepts are needed to improve the cooling performance. Liquid jet impingement cooling [2] is regarded as an effective cooling technique for high power electronics due to the high local cooling rate, better temperature uniformity and lower pressure drop compared with microchannel coolers. In literature studies, this cooling technique has been applied on the power module baseplate [3], on the substrate [4] or even on the bare die [5,6,7]. Among these techniques, bare die liquid jet impingement cooling with locally distributed outlet returns is regarded as the most efficient cooling option where the liquid coolant is directly ejected from nozzles on the device backside resulting in a high cooling efficiency due to the absence of the thermal interface materials (TIM) and the lateral temperature gradient. Moreover, a lower pressure drop can be realized since the outlet flow within the cooling unit cell can be removed locally whereas the pressure drop of

* Corresponding author.
E-mail address: tiwei.wei@imec.be (T.-W. Wei).

https://doi.org/10.1016/j.applthermaleng.2020.115767
Received 10 February 2020; Received in revised form 25 June 2020; Accepted 17 July 2020
Available online 21 July 2020

Nomenclature

A	Chip Area, [mm^2]
d_i	Inlet Nozzle diameter, [μm] or [mm]
d_o	Outlet Nozzle diameter, [μm] or [mm]
d_i/L	Nozzle Diameter Ratio, -/-
f	Pressure Coefficient
H	Cavity Height, [mm]
$H_{critical}$	Critical Cavity Height, [mm]
L	Nozzle Pitch (cooling unit cell length), [mm]
N^2	Total number of inlet nozzles
Nu	Nusselt Number
N^2/A	Nozzle Density, [cm^{-2}]
P_{in}	Inlet Pressure, [Pa]
P_{out}	Outlet Pressure, [Pa]
Q_{hs}	Heat Generated in the Heater Cells, [W]
R_{th}^*	Normalized Thermal Resistance, [cm^2-K/W]
Re	Reynolds Number
T_{avg}	Average Junction Temperature, [°C]
T_{in}	Coolant Inlet Temperature, [°C]
t	Nozzle length, [mm]
$\dot{V}_n$	Flow Rate per Nozzle, [ml/min]
$\dot{V}$	Total flow rate for all the nozzle arrays, [ml/min]
Wp^*	Normalized Pumping Power, [W/cm^2]
ΔP_{tot}	Pressure Difference between Inlet and Outlet, [Pa]
Δp_{ch}	Pressure Drop across the cavity height, [Pa]
Δp_{nz}	Pressure Drop across the jet nozzle, [Pa]
Δp_{jet}	Pressure Drop generated by Jet Cooling, [Pa]
Δp_{loss}	Pressure loss of Flow Expansion and Flow Contraction, [Pa]

Subscripts

avg	average
ch	channel
i/in	inlet
o/out	outlet
hs	hotpots of the heater
n	nozzle
p	pumping
tot	total
th	thermal

Acronyms

COP	Coefficient of Performance
BEOL	Back-end of Line
CAD	Computer-aided Design
CFD	Computational Fluid Dynamics
DI	Deionized
DOE	Design of Experiment
FL	Flow Rate
FS	Percentage of Full Scale
GCI	Grid Convergence Index
IGBT	Insulated-Gate Bipolar Transistor
MOSFET	Metal–Oxide–Semiconductor Field-Effect Transistor
PCB	Printed Circuit Board
PTCQ	Packaging Test Chip Version Q
QUICK	Quadratic Interpolation for Convective Kinetics
RD	Percentage of Reading
SIMPLE	Semi-Implicit Method for Pressure-Linked Equations
SLA	Stereolithography
SST	Shear Stress Transport
TIM	Thermal Interface Materials

microchannel cooling is scaling with the channel length.

In [8,9], a systematic review about microjet cooling techniques is presented and the thermal performance is benchmarked. Fig. 1 summarizes the published performance data in terms of the reported heat transfer coefficient as a function of the jet nozzle density, where the nozzle density is defined as the total nozzle number divided by the cooled chip area, shown as N^2/A. In general, the chart shows an increase of the heat transfer for high nozzle density values. However, the highest achieved heat transfer is not obtained from the finest nozzle array. Furthermore, high nozzle densities require more expensive fabrication techniques, such as the silicon and ceramic fabrication techniques, due to the complexity of the internal structure and the integration with the chip packaging. Therefore, a thorough investigation of the impact of the nozzle density is very important for the design of an efficient liquid impingement jet cooler and the selection of a cost-efficient fabrication technique.

Several studies showed the demonstrations and measurements for different nozzle densities, based on jet nozzles with distributed returns. In [3], a metal based single-jet direct impingement cooler with nozzle density of 1.56 cm^{-2} was demonstrated on a single MOSFET semiconductor showing a heat transfer coefficient of 1.2×10^4 $W/(m^2 K)$ for a pumping power of 0.9 W. However, the obtained heat coefficient distribution for single jet cooling is highly nonuniform, due to the different flow regions: stagnation region, wall jet region and decay region. In [6], Brunschwiler et al. demonstrated that Si based microjet array impingement coolers with 50,000 inlet/outlet nozzles, allow to increase the heat transfer coefficient to 8.7×10^4 $W/(m^2 K)$ with 1.43 W pumping power. The nozzle density of this cooler is 12,500 cm^{-2}. Moreover, Natarajan and Bezama [7] developed a microjet cooler with 1600 inlets and 1681 outlets using multilayer ceramic technology, resulting a nozzle density of 888 cm^{-2}. The main drawbacks of the Si or ceramic based coolers are the high pressure drop for the small diameter nozzles and the high fabrication cost. In our previous studies, polymer based 4×4 jet array coolers with nozzle density of 25 cm^{-2} and nozzle diameter of 0.6 mm were demonstrated with micromachining [9] and stereolithography 3D printing [19]. The multi-jet cooler with a nozzle

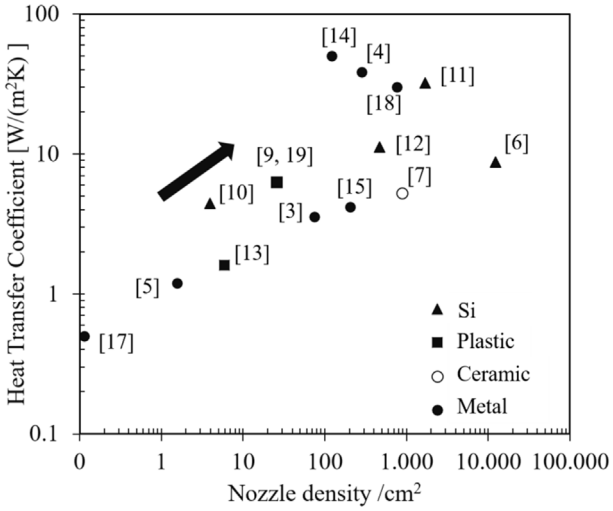

Fig. 1. Trend of the dissipated heat flux in the chip as a function of the nozzle density of the cooler ().
adapted from [9] (See above-mentioned references for further information.)

density of 25 cm^{-2} can achieve heat transfer coefficients up to 6.25×10^4 $W/(m^2 K)$ with a pumping power as low as 0.3 W. However, the manufacturability of a micro-machined cooler is limited by the critical parameter of the drilling and milling tools.

The thermal performance of the cooler is furthermore affected by the nozzle diameter d_i and cavity height H which are usually coupled with the nozzle density N^2/A. For a free-surface jet cooling, Womac et al. [20] observed that the H/d_i ratio had a negligible effect on the heat transfer based on the experimental study. For the single submerged and the confined jet cooling, Garimella [21,22] experimentally investigated the effect of H/d_i, L/d_i, and the flow rate on heat transfer. They found that H/d_i significantly affects the heat transfer performance of the system, especially for multiple confined jet impingement cooling. Al-dabbagh and Sezai [23] also concluded that cavity height (H) significantly affects heat transfer performance. Afzal Husain [24] reported that at both low and high flow rates, the change in cavity height does not affect the pressure drop significantly. However, the decrease in the spacing between the nozzle to the heated surface increases the heat transfer coefficient monotonously.

Brunschwiler et al. defined four typical regimes based on the cavity height, which are the pinch-off regime ($H < H_{critical}$), the impingement regime, the transition regime, and the separation regime [6]. They observed that both the heat transfer and the pressure drop increase rapidly for reducing cavity height in the pinch-off regime and that the heat transfer remains constant as a function of the cavity height in the impingement regime. In [25], the experimental study also showed that the thermal performance was insensitive to the gap at large spacing, but below a specific gap it degraded with decreasing gap. However, the studies are only limited to a specific nozzle density. From the discussion above, it is clear that there is an interaction between the impact of the nozzle density and the cavity height on the thermal and hydraulic performance of the impingement jet cooler.

The focus of this paper is to investigate the combined impact of the jet array design parameters on the thermo-hydraulic cooler performance. These parameters are: 1) the nozzle density, 2) the cavity height, and 3) the nozzle diameter. This paper first shows the design and fabrication of demonstrators for three different nozzle densities with a 3 × 3, 4 × 4, and 8 × 8 nozzle array fabricated using 3D printing. In section III, the impact of the nozzle density on the thermal and hydraulic performance will be investigated experimentally. In section IV, a conjugate heat transfer and fluid flow Computational Fluid Dynamics (CFD) unit cell modeling approach is introduced and experimentally validated. In the last section, the validated model is applied to assess the combined thermal impact of the nozzle density on nozzle diameter and cavity height on the thermo-hydraulic performance through an extensive design of experiments. The objective of this study is to provide guideline for predicting the thermal/hydraulic performance of the cooler based on user's constraint working conditions.

2. Demonstration of 3D printed cooler with different nozzle density

2.1. Design of the microjet cooler

The schematic of the microjet cooler with distributed returns is illustrated in Fig. 2. The inlet manifold is used to distribute the cold coolant over the N × N array of inlet nozzles. The nozzle arrays consist of several unit cells. The latter are defined as cooler units with a single inlet in the center and four outlets located at the four corners. After the fluid impinges onto the chip backside, the outlet manifold collects the flow and evacuates the coolant through the outlet nozzles of an (N + 1) × (N + 1) array.

Stereolithography (SLA) can achieve a high resolution in the micrometer range (for example 1 μm in Z direction (layer thickness) and a few to tens of microns in XY direction (pixel size) by using photopolymers. Based on the manufacturability of the SLA technology, three different versions of the jet impingement cooler are designed for the bare die thermal test chip package that contains an 8 × 8 mm^2 thermal test chip [27]. Fig. 3 shows cross-sections of the design of the coolers with a 3 × 3, 4 × 4 and 8 × 8 inlet nozzle array. Therefore, the maximum nozzle density for the cooler demonstration is 100 cm^{-2}. For this study on the impact of the nozzle density, the geometrical parameters of the inlet and outlet plenum level are all kept fixed. The inlet chamber is designed as 2.5 mm and the cavity height for the three full coolers is designed as 0.6 mm. Moreover, the nozzle diameter ratio d_i/L defined as the nozzle diameter over the inlet nozzle pitch L is kept fixed at 0.3 [see Table 1].

2.2. Cooler fabrication and assembly

The stereolithography SLA printing equipment Formlabs Form 2 with high resolution of 0.13 mm for the XY draw plane and 0.406 mm for the Z build direction, is used in this study. With the high-resolution SLA, the coolers with 3 × 3, 4 × 4 and 8 × 8 nozzle arrays are successfully printed using one single process without assembly of the individual parts. The bottom view of different fabricated coolers is illustrated in Fig. 4. Moreover, the 3D reconstructed microscope images are also shown in Fig. 4. It can be seen that all nozzles are functional with no blockages or trapped resin observed even for smallest 8 × 8 nozzle array design. Fig. 5 shows the distribution of the measured nozzle diameter for the different nozzle arrays. In general, the actual nozzles diameters are within 18% difference from the nominal design values for 4 × 4 and 8 × 8. However, a difference of 26% is found for 3 × 3 with a nominal nozzle diameter of 800 μm. This is due to the higher measurement uncertainty for the small nozzle diameter with relatively larger roughness. The fabricated larger nozzle diameter is expected to have a higher thermal resistance under the same flow rate, but exhibit a lower pressure drop (larger diameters) and therefore will require a lower pumping power. The fabrication tolerance and impact of the

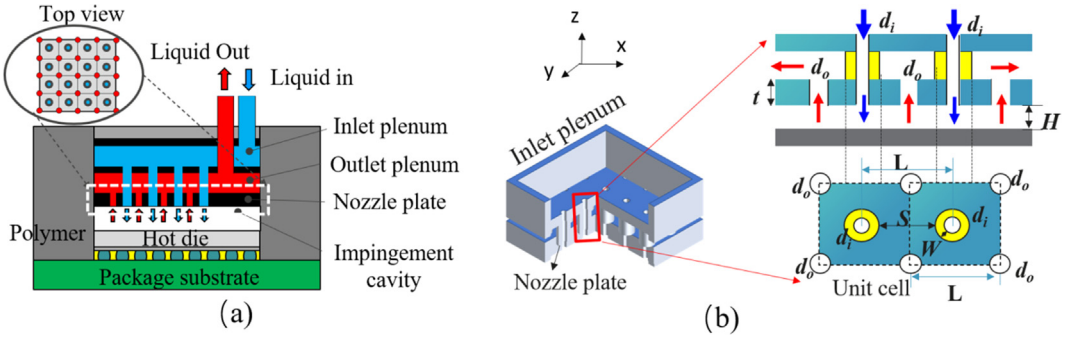

Fig. 2. Schematic of the microjet array cooling: (a) cross section view of the full nozzle array with inlets and outlets; (b) geometry parameters definitions (schematic). adapted from [26]

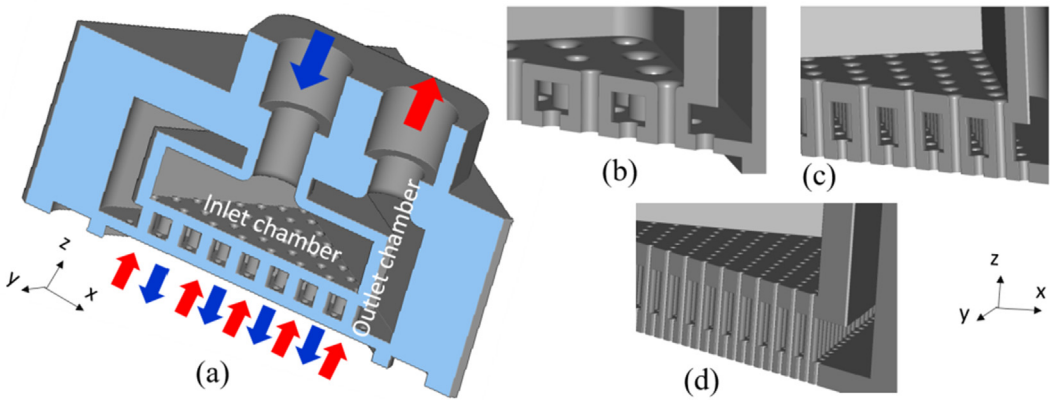

Fig. 3. CAD (Computer-aided design) structures: (a) 8 × 8 array cooler with inside channels and enlarge view for three different nozzle array (b) 3 × 3 (c) 4 × 4 and (d) 8 × 8.

Table 1
Nozzle density with respect to the 8 × 8 mm^2 test chip with d_i/L = 0.3.

Symbol	N×N	Nozzle density (cm^{-2})	Cooling unit cell (mm)	Nozzle diameter (mm)
N1	1×1	1.56	8	2.4
N2	2×2	6.25	4	1.2
N3	3×3	14.06	2.6	0.8
N4	4×4	25	2	0.6
N6	6×6	56.25	1.33	0.4
N8	8×8	100	1	0.3
N12	12×12	225	0.67	0.2
N16	16×16	400	0.5	0.15
N20	20×20	625	0.4	0.12
N32	32×32	1600	0.25	0.08

printing tolerance was investigated in our previous study [10].

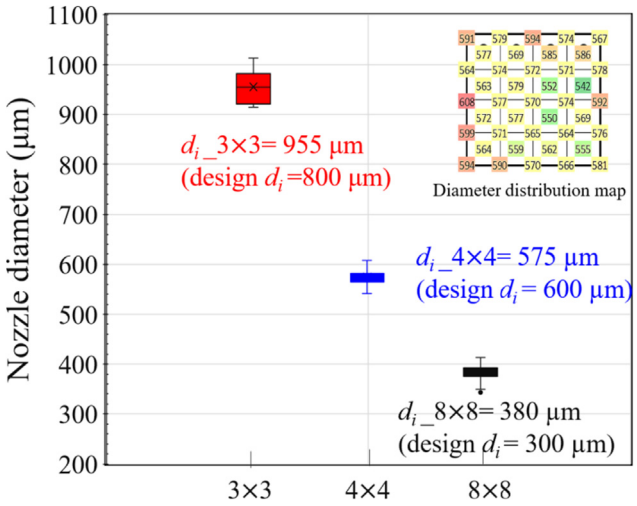

Fig. 5. Nozzle diameter statistics with different nozzle array.

3. Experimental analysis of nozzle scaling trend

3.1. Experimental set-up

In order to characterize the thermal and hydraulic performance of

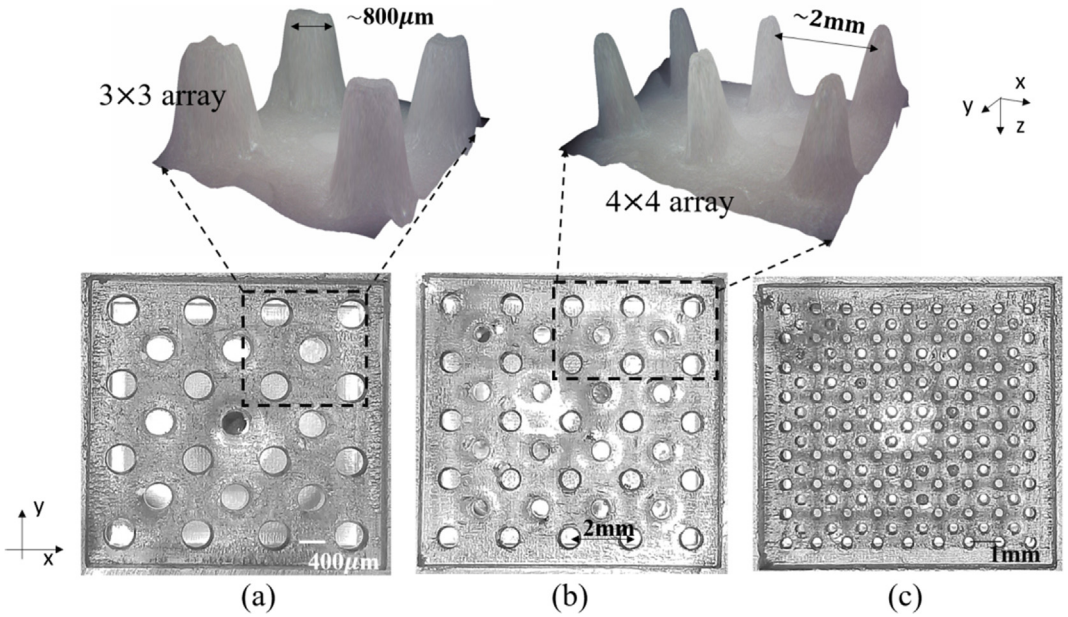

Fig. 4. 3D reconstructed microscope images (top) and bottom view of the nozzle plate (bottom) of the fabricated 3D printed coolers: (a) N3: 3 × 3 (b) N4: 4 × 4 and (c) N8: 8 × 8.

the cooler, a dedicated closed loop temperature measurement and pressure drop measurement system [9] is used, shown in Fig. 6. The fluid used in this measurement is Deionized water (DI water). The flow rate in the system is controlled by a mini Cori flow meter with accuracy of ± 0.2% as a percentage of reading (%RD). The pressure drop between the inlet and outlet is measured by a differential pressure gauge that can withstand a static pressure of 10 bar. The scope of the pressure drop is between 0.2 and 5 bar with an accuracy < ± 0.5% as a percentage of full scale (% FS). A stainless-steel basket filter is used for the pump with a screen of 25 μm. The thermal measurement set-up system is shown in Fig. 7. The cooler with 8.6 mm × 14 mm × 14 mm volume size is fixed on the organic package substrate where the nozzle arrays are located on top of the Packaging Test Chip Version Q (PTCQ) thermal test chip [27].

The programmable 8 × 8 mm^2 thermal test chip contains a 32 × 32 array of temperature sensors to measure the full chip temperature distribution map. The details of the thermal test chip are shown in Fig. 8. As illustrated in Fig. 8(a), the flip-chip package of the bare die is soldered on the printed circuit board (PCB) test board, allowing the control of the temperature sensor diodes and resistor heaters. The heaters are constituted by metal meanders resistors in the backend of line (BEOL) that are controlled independently, resulting in a customizable programmable power map with 832 heater cells with 75% heater uniformity, shown in Fig. 8(b). As shown in Fig. 8(c), the chip with an area of 8 × 8 mm^2 contains a 32 × 32 array of 240 × 240 μm^2 square cells with additional peripheral circuits with I/O and control cells in the central cross of the chip. The used temperature sensor, in the center of each cell, is a diode, for which the voltage drop across diode at fixed DC current can be used as the measure of temperature. This diode, with a size of 4.8 μm × 2.6 μm is shown in Fig. 8(d). The chip temperature distribution thus can be measured with a spatial resolution of 240 μm, allowing the accurate capturing of local temperature effects on the chip. The measurement uncertainty for the sensor and heater voltage are 1 mV and 1.6 mV respectively. The 95% confidence interval of the calibrated sensitivity of the temperature sensor on the test chip is − 1.55 ± 0.02 mV/°C in the temperature range between 10 and 75 °C for a current of 5 μA. The analysis of the propagated measurement uncertainty results in a value of ± 1.8% for the reported thermal resistance measurements.

3.2. Characterization metrics definitions

In order to characterize the thermal and hydraulic performance of the cooler, the characteristic metrics are defined and explained in this section. First, the nozzle density in this study is defined as follows:

$$\rho_N = N2/A \quad (1)$$

Since the thermal performance of the cooler scales with the chip area, the thermal resistance R_{th}^* is normalized as follows [19]:

$$R_{th}^* = A(T_{avg} - T_{in})/(Q_{hs}) \quad (2)$$

where the Q_{hs} is the heat generated in the heater cells based on the measured electrical current and heater voltage. The total pressure drop ΔP_{tot} is defined as the pressure difference between inlet pressure P_{in} and outlet pressure P_{out}:

$$\Delta P_{tot} = P_{in} - P_{out} \quad (3)$$

The normalized pumping power Wp^* is expressed as follows:

$$Wp^* = \dot{V}\Delta P_{tot}/A \quad (4)$$

Therefore, the normalized pumping power will be independent of the chip area, for equal flow rates per nozzle.

3.3. Thermal/Hydraulic measurements

The thermal performance measured by the thermal test chip with the three different coolers is shown in Fig. 9 for a constant flow rate (FL) of 1000 ml/min. It can be seen that the chip temperature reduces with increasing nozzle density. The observed trend with increasing cooling performance can be concluded as N3 < N4 < N8. The temperature profile along the chip diagonal is also compared in Fig. 9(d). The comparison shows that a very good thermal performance R_{th}^* of 0.13 cm^2K/W for the 8 × 8 cooler with 1 × 1 mm^2 cooling cells can be achieved.

The experimental results in Fig. 10 show that the thermal resistance reduces when the nozzle density increases from 14 cm^{-2} to 100 cm^{-2}. In this study, the nozzle density is limited to 100 cm^{-2} based on the current limitations on the 3D polymer printing technology. To extrapolate the thermal performance, a conjugate heat transfer and fluid flow CFD unit cell model is used to further investigate this scaling trend for the nozzle density up to 1600 cm^{-2}, corresponding to a 32×32 nozzle array on the 8×8 mm^2 test chip. It was shown previously that the unit cell CFD model, extracted from the full N×N nozzle array is an efficient and accurate method to study the thermal and hydraulic performance of an impingement cooler, as demonstrated for a 4×4 jet array cooler [6]. In the next section, the details of the unit cell model and modeling methodology will be introduced and validated.

4. Modeling methodology and validation

The unit cell modeling domain, shown in Fig. 11, corresponds to 1/8 of one liquid cooling unit cell (Fig. 2b), which consist of a central inlet nozzle surrounded by four outlet nozzles. ANSYS Fluent 18.0 is used for the CFD modeling. The unit cell modeling approach is based on the assumption that there is no pressure gradient in the full N×N nozzle array. The ΔP_{tot} is defined as the pressure difference between inlet and outlet nozzle. The boundary condition for every inlet nozzle is set at a constant velocity. The static pressure for the outlets is set at 0 Pa. The fluid/solid wall on each side is considered as a symmetry boundary. A constant heat flux is applied on the chip bottom to represent the heating in the test chip. The coolant inlet temperature is set at a constant temperature value of 10 °C.

The mesh is performed in the ANSYS fluent mesh module. The governing equations in the numerical simulation are the momentum and energy equations, defined in ANSYS. For the meshing of the unit cell shown in Fig. 11(a), tetrahedral meshing cells are used in the fluid domain. The first layer thickness for the boundary layer along the fluid wall is 1 μm to make sure the grid is fine enough to get y + <1 in the viscous sublayer in case of the 600 μm nozzle. For the cases with a high nozzle density, the mesh is scaled in order to keep a constant ratio between the element size and the nozzle diameter. For the unit cell model, extensive design of experiments are performed for the

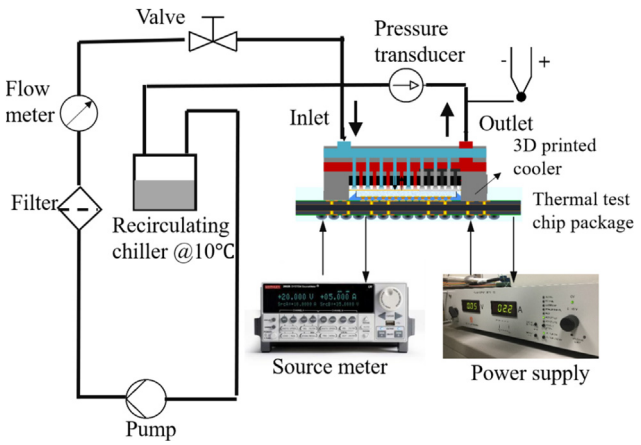

Fig. 6. Schematic of the flow loop measurements system with pressure and flow rate control.

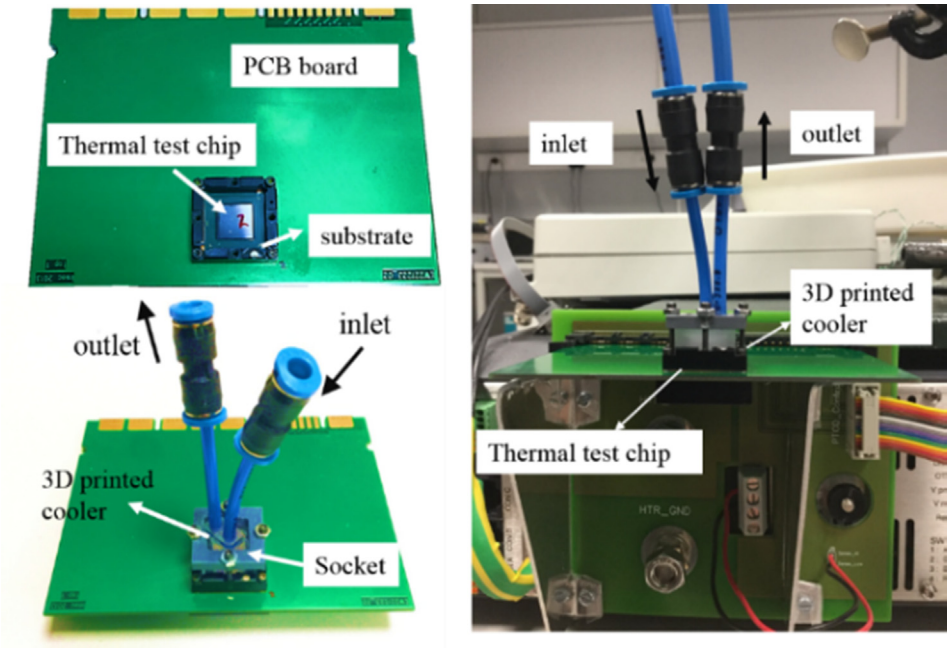

Fig. 7. Cooler assembly and experiment set up for the temperature measurement of the microjet cooling.

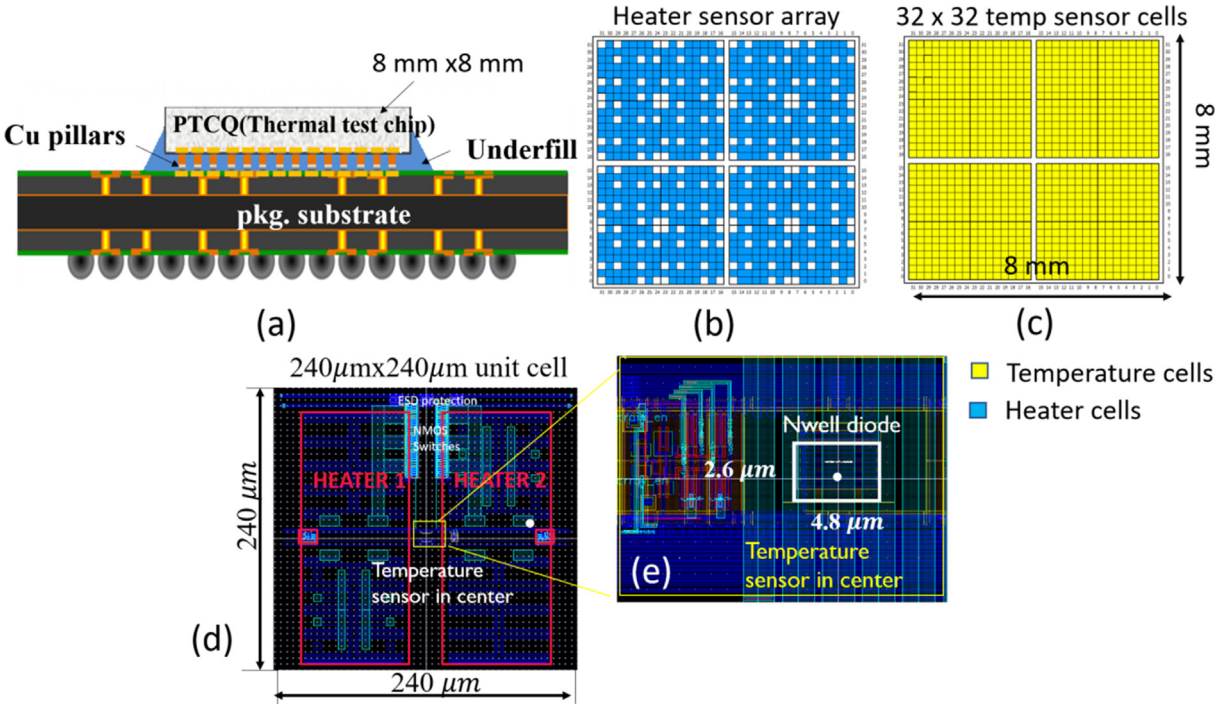

Fig. 8. Introductions of the PTCQ thermal test chip: (a) thermal test chip package schematic; (b) layout of one heater cell; (c) indication of one temperature sensor (diode sensor); (d) and (e) dimensions and structure details of the diode temperature sensor.

dimensionless analysis and parametric analysis. Therefore, meshing sensitivity is needed to make sure the modeling results are mesh independent. Table 2 lists the grid convergence index (GCI) analysis for different nozzle array for a fixed cavity height. The final chosen mesh size is between 0.005 mm and 0.02 mm for the nozzle array from 4×4 to 32×32, resulting the element number between 0.6 million to 1 million in the computation domain.

For the numerical scheme, the Semi-Implicit Method for Pressure-Linked Equations (SIMPLE) algorithm is used as the solution method while the Quadratic Interpolation for Convective Kinetics (QUICK) scheme is chosen for the numerical discretization. The convergence criteria were set at 10^{-5} for continuity, 10^{-6} for energy and 10^{-6} for k, ω and momentum (x, y and z components of velocity), respectively.

For the studied flow rate range from 100 ml/min to 1000 ml/min, the corresponding Reynolds number, based on the jet diameter, is between 50 and 2000. Since the laminar to turbulent transition for jet impingement flows occurs for Re_d numbers between 1000 and 3000 [8], the coolant flow is expected to be in the laminar regime or the transition regime for the considered cases. To cover both regimes in the CFD model, a transition Shear Stress Transport (SST) model is used for the simulations. In our previous study [32], the transition SST model has been validated with a reference Large Eddy Simulation (LES) model

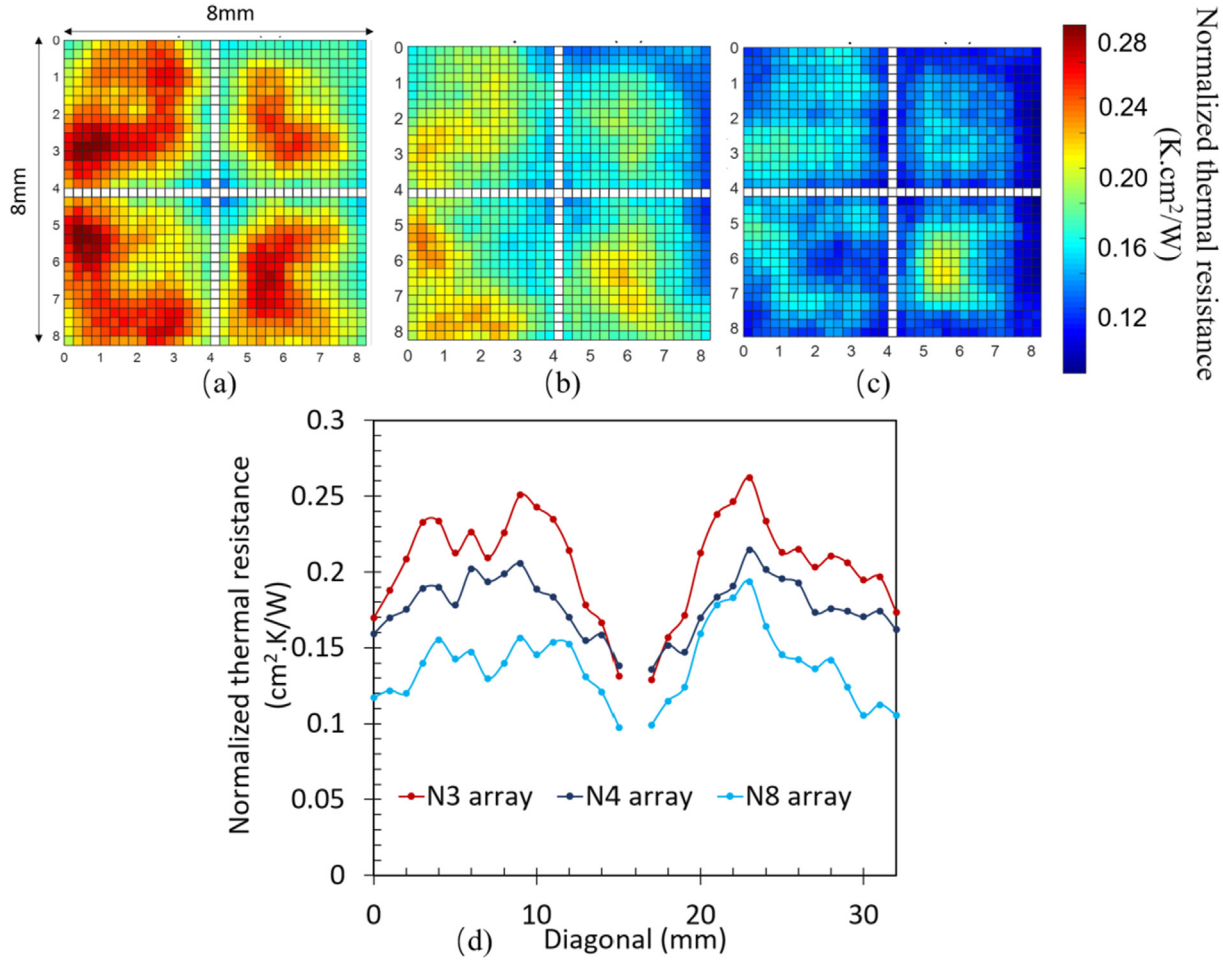

Fig. 9. Comparison of the temperature distribution for (a) 3 × 3 (b) 4 × 4 and (c) 8 × 8 nozzle array; (d) temperature profiles comparison along the chip diagonal (H = 0.6 mm, Q_{hs} = 40 W, FL = 1000 ml/min).

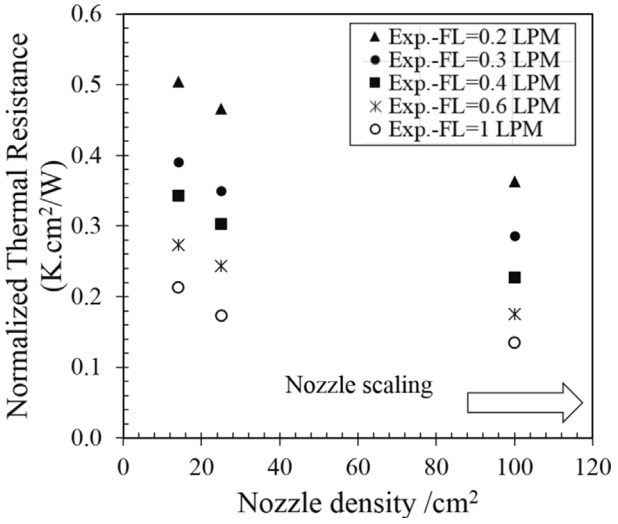

Fig. 10. Experimental results expressed as normalized thermal resistance as a function of the nozzle density for three different nozzle density values 14.06 cm^{-2}, 25 cm^{-2} and 100 cm^{-2}.

for the same unit cell geometry. It was shown that the transition Shear Stress Transport (SST) model shows excellent ability to predict the stagnation Nu number and the average Nu number, as well as the local level pressure coefficient f with less than 5% difference in the range of $30 < Re_d$ less than 4000, compared with the reference LES model. This justifies the use of the faster transition SST model in the extensive design of experiments with a high level of confidence, instead of the time consuming LES model.

In Fig. 11, the unit cell model schematic with the boundary conditions and solid–fluid domain are indicated. The flow boundary conditions are declared in the inlet and outlet, as illustrated in Fig. 11(b). The final mesh of the unit cell model for 4×4 nozzle array with nozzle diameter of 0.6 mm is shown in Fig. 11(c). The material properties are listed in Table 3.

The flow regions and temperature distribution for unit cell modeling results for a flow rate of 1.47 m/s is shown in Fig. 12. The applied heat flux is 37.5 W/cm^2. From the flow streamline, the jet flow behaviors can be observed in Fig. 12(a). Moreover, it is found that the lowest temperature is in the stagnation region of the jet flow, as indicated in Fig. 12(b).

The comparison between the experimental measurements and the results of the CFD unit cell model is shown in Fig. 13. A good agreement can be observed between the modeling and experimental results. Therefore, the CFD model with the unit cell approach is successfully validated, and it can be used for the extrapolation of the thermal performance for higher nozzle densities beyond 100 nozzles per cm^2. As discussed in Fig. 13, the experimental results show that there is a decrease of thermal resistance when the nozzle density increases from 14 cm^{-2} to 100 cm^{-2} for a fixed cavity height and diameter ratio. Using the validated model, this analysis can be generalized for a large range of cavity heights and diameter ratios. The range of dimensions are listed in Table 4.

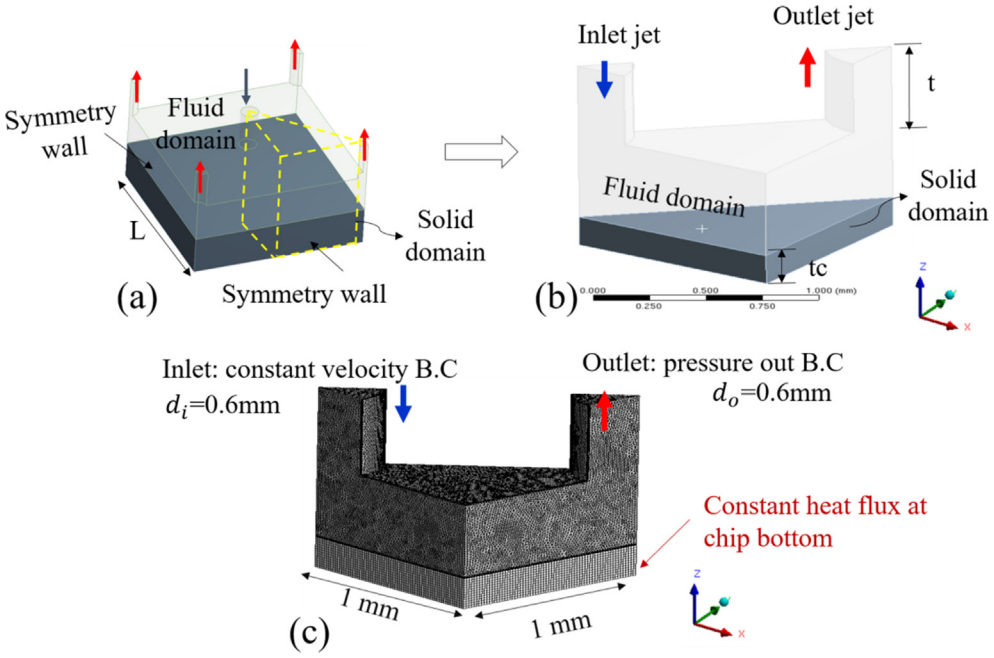

Fig. 11. Unit cell model for 4×4 nozzle array: (a) one quarter model of the full nozzle array; (b) 1/8 model: unit cell model; (c) meshing details of the unit cell model.

Table 2
GCI analysis for the unit cell model with different nozzle array (d_i/L = 0.3, H = 0.6 mm, V_{in} = 1.47 m/s).

Nozzle array	Mesh size (mm)	GCI_{12}	Asymptotic range of convergence
4 × 4	0.02	0.0000	1.0000
6 × 6	0.02	−0.0002	0.9990
8 × 8	0.01	0.0002	0.9999
10 × 10	0.01	−0.0013	0.9994
12 × 12	0.005	0.0001	1.0000
20 × 20	0.005	0.0008	0.9995
32 × 32	0.005	0.0008	0.9991

Table 3
Dimensions and Material properties.

Material	Specific heat [J/(kg K)]	Thermal conductivity
Si	556.9	149 W/m K
Water	4182	Piecewise-linear, Temperature dependent

As shown in Fig. 13(b), there are two opposing trends observed for the pressure drop as a function of the number of nozzles: for low nozzle density values, the pressure drop between the inlet and the outlet of the unit cell is dominated by contribution from the cavity region; for nozzle density values, the pressure drop inside the inlet andoutlet nozzles dominates. Specifically, the pressure drop reduces significantly with the increase of the nozzle density up to 25 cm^{-2}. This can be explained due to the fact that the pressure drop contribution for the channel flow in the cavity region Δp_{ch} decreases due to the reduction of the distance between inlet and outlet of each unit cell for an increase of the nozzle density and the corresponding reduction of the unit cell dimensions. It can be observed, that this leads to a high cooler pressure drop for the extreme case of the single jet cooler, where the unit cell length is equal to half of the chip size. However, this trend of the pressure drop reduction turns to go up at certain point (25 cm^{-2}) as the nozzle density keeps growing. This is mainly due to the dominant contribution of pressure drop Δp_{nz} inside inlet and outlet nozzles from that point on. Indeed, the Δp_{nz} goes up with the reduction of the nozzle diameter due to the increasing nozzle density. The total pressure drop becomes very high for larger nozzle arrays due to the smaller nozzle diameter with high aspect ratio, for a constant flow rate. These trends are discussed in more detail in section 5.3.1.

5. Nozzle scaling analysis with validated model

5.1. Criteria for comparison

The objective of this study is to find the best combination of the design variables and study the scaling trends. An extensive parameter sensitivity study has been performed by varying the three variables: nozzle density: N^2/A, cavity height H and nozzle diameter ratio d_i/L. The parameters and their range are listed in Table 4.

The outputs of the model are the thermal resistance and pressure drop or pumping power as introduced in Section 3.2. In order to compare the cooling performance for different cooler geometries, there are mainly two criteria for the comparison.

The first option is to compare the thermal performance at a constant flow rate, since the flow rate is a typical system level parameter for the closed loop cooling and limited by the pump. For a smaller nozzle diameter, a larger velocity per nozzle is needed for the same flow rate, resulting in higher pressure drop and pumping power. Therefore, the trade-off between the thermal resistance and pumping power should be taken into account in this analysis. A metric that can be used to include both aspects, is the coefficient of performance (COP) [29,30,33], defined as the ratio between the cooling power and the required pumping power. In the context of the impingement cooling, the COP can be defined as follows:

$$COP = \frac{Cooling\ \ Power}{Required\ \ pump\ \ power} = \frac{Max\ \ allowed\ \ temp\ \ increase/Rth}{Required\ \ pump\ \ power} \quad (5)$$

Therefore, the beneficial effect of the thermal resistance and the detrimental effect of the pressure drop can be combined, where a higher COP indicates a better cooler design. The definition of the general COP is defined as the desired heat power divided by the required pumping power, where the required pumping power includes the chiller power, and fluidic tube connection consumed power. It should be noted that the COP defined in this paper only includes the required pumping power related to the pressure drop between the cooler inlet and outlet, while the system level tube connections, chiller power, and others are

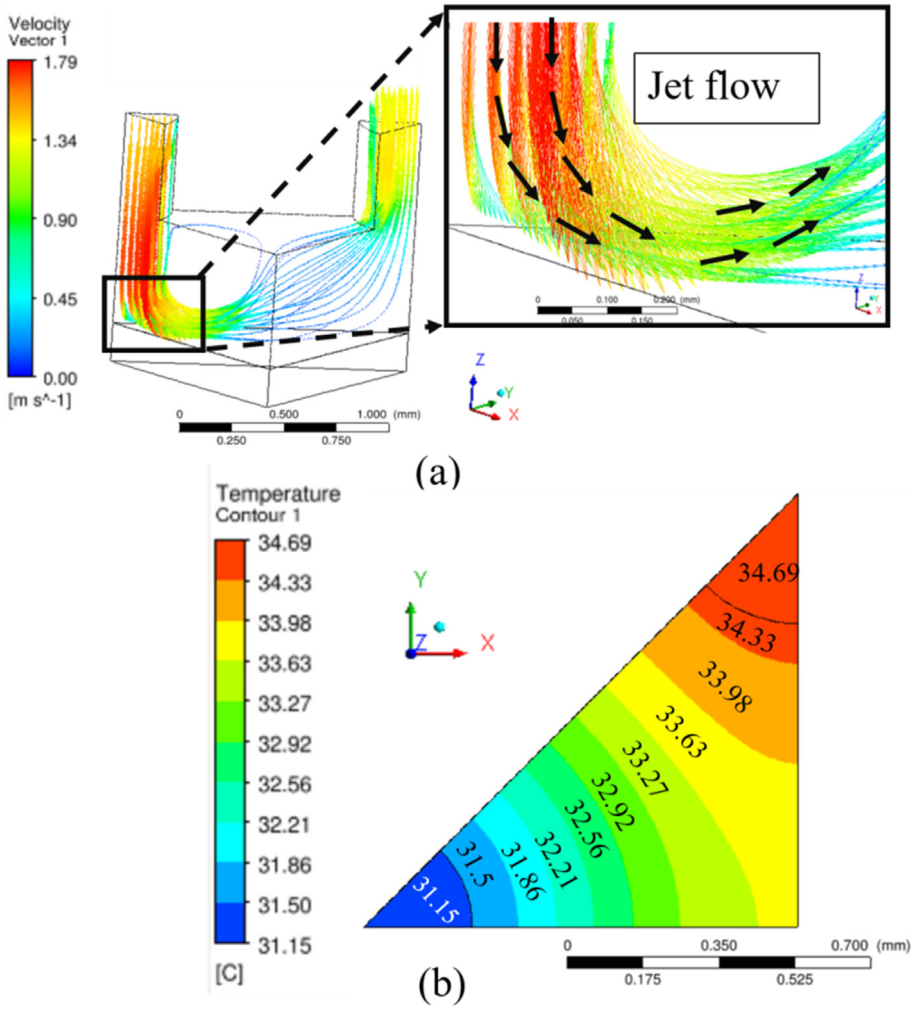

Fig. 12. Unit cell modeling results: (a) flow streamline with arrows; (b) temperature contour on the chip surface under heat flux of 37.5 W/cm^2. (V_{in} = 1.47 m/s, T_{in} = 10 °C).

not taken into account, resulting in an artificially high value for the reported COP. The reason is that we want to perform a relative thermo-hydraulic performance comparison of different cooler design parameters, following the methodology introduced in [33].

The second option is the comparison for a constant pumping power. For smaller nozzle diameters, the pressure drop is higher for a constant flow rate. Therefore, a smaller flow rate needs to be used to maintain a constant pumping power. By comparing the thermal performance at a constant pumping power, the energy efficiency of the coolers is compared, which determines how much heat is removed for the same required pumping power, taking into account the hydraulic aspects.

5.2. Single variable analysis

5.2.1. Fixed cavity height

Fig. 13 shows the improvement of thermal performance and an increase of the pressure drop for increasing nozzle density for constant flow rate and cavity height. The trade-off is shown in Fig. 14 in terms of the COP, plotted as a function of nozzle density and nozzle diameter for a fixed flow rate of 600 ml/min and a cavity height fixed at 200 μm. The parameters d_i/L and N^2/A are varied according to Table 2. As the nozzle density increases, the COP first increases very fast until the range around 100–200 cm^{-2} and then the COP decreases slowly. It can also be observed that the higher inlet diameter ratio, the larger the COP is. The impact of the nozzle diameter ratio is larger than the impact of the nozzle density. At a nozzle density of 100 cm^{-2} (8×8 array), the COP for d_i/L = 0.4 and 0.3 are respectively 100 and 40 times higher than the COP for d_i/L = 0.1, while the difference between the COP for N^2/A = 1 and 100 is a factor of 13 for a constant d_i/L = 0.3. Therefore, the comparison indicates that the nozzle diameter is the dominant parameter for the thermal performance of the jet impingement cooling, where the d_i/L ratio should be chosen as high as possible. The d_i/L ratio is limited by the unit cell configuration ($0 < d_i/L < \frac{\sqrt{2}}{2}$) and by the consideration to maintain sufficient structural rigidity of the nozzle plate. Therefore, the value of d_i/L = 0.3 is chosen as a reference value for the nozzle diameter, even when higher values for d_i/L still further improve the COP.

5.2.2. Cavity height impact

In order to better understand the thermal and hydraulic behavior of the cooler, the temperature increase and pressure drop as a function of the different cavity heights are plotted in Fig. 14, assuming a constant flow rate of 600 ml/min and a diameter ratio of d_i/L = 0.3. It can be seen that the temperature increases rapidly as H decreases when the cavity height is below 0.1 mm. This phenomenon can be explained by the “Pinch-off regime” observed by Brunschwiler et al. [6]. For the pinch-off regime with very thin cavity height, the pressure drop is very high since the flow is confined inside the thinner cavity channel. As the cavity height is higher than H = 0.2 mm, the flow regime moves to the “impingement” regime, where the heat transfer performance and pressure drop both keep stable.

Besides, it is also observed that the average temperature for

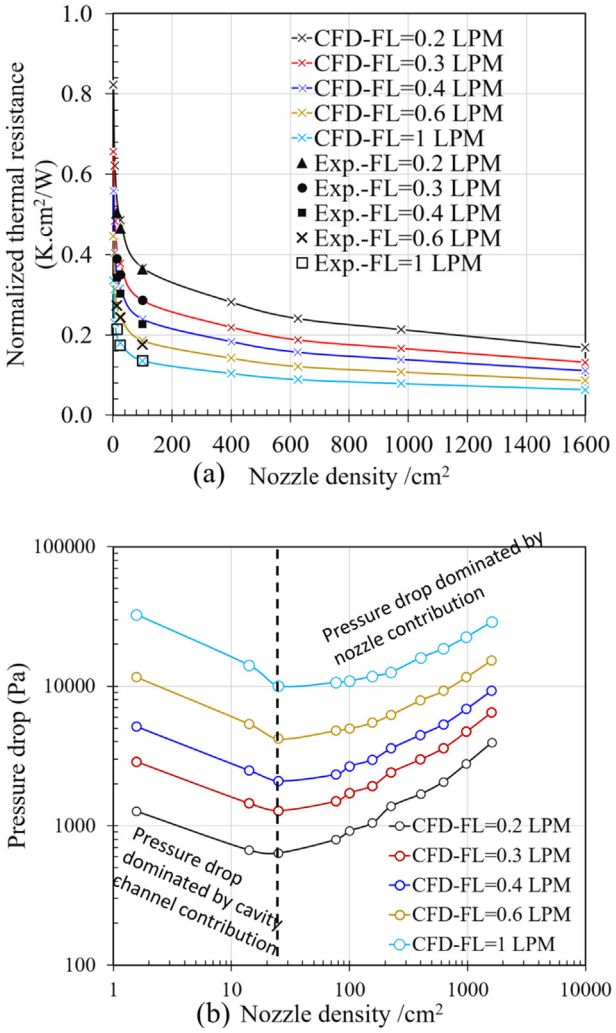

Fig. 13. Experimental validation of the nozzle scaling trend on the (a) normalized thermal resistance and (b) pressure drop with the unit cell modeling approach (cavity height H = 0.6 mm, constant nozzle diameter ratio d_i/L = 0.3).

Table 4
List of parameters and range.

Parameter	Symbol	Values
Nozzle density	N^2/A	1.56; 14; 25; 76.56; 100; 156; 225; 400; 625; 1600 cm^{-2}
Cavity height	H	0.01:0.01:1 mm
Nozzle diameter ratio	d_i/L	0.025; 0.05; 0.1; 0.2; 0.3; 0.4

different nozzle densities are very close to each other in the "pinch-off" regime, shown in Fig. 15(a). This behavior is consistent with the results shown in Fig. 13(a), that the thermal performance will be saturated with the increment of the nozzle density. However, there is a large temperature difference in the "impingement" regime, showing that the higher nozzle density can achieve lower chip temperature for a constant flow rate.

As for the pressure drop in the "pinch-off" regime shown in Fig. 15(b), the higher nozzle density (N = 32) shows lower pressure drop. This is due to the short nozzle pitch L for higher nozzle density. The short channel length L along the wall jet region results in a pressure drop decrease in the thinner cavity channel, which is the dominating factor for the overall unit cell pressure. However, this trend changes inversely in the "impingement" regime, showing that the higher nozzle

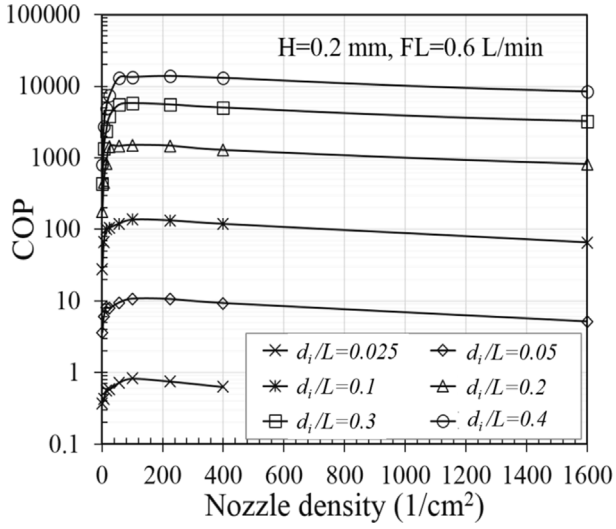

Fig. 14. The thermal impact COP as function of the nozzle density, under the constant cavity height (H = 0.2 mm, FL = 0.6 L/min).

density can generate higher pressure drop. This is because the pressure in this regime is dominated by the nozzle channel pressure, where the nozzle diameter for higher N is very small.

In general, it can be seen that there are two different trends for the variation of the cavity height, from thermal and hydraulic point for view. In the next section, the interactions between the impact of the nozzle density and the cavity height on the thermal and hydraulic performance of the impingement jet cooler will be discussed.

5.3. Combined impacts

In Section 5.2.1, the investigation of the single variable shows that the inlet nozzle diameter is the dominant parameter, which should be optimized first. Next, the combined impact of nozzle density and cavity height are studied in this section.

5.3.1. Comparison 1: Constant flow rate

The final design of experiment (DOE) results with the combined effects of the nozzle density and cavity height on the COP are summarized in Fig. 15, for a flow rate of 0.3 L/min and 0.6 L/min. The opposing trends for the thermal and hydraulic performance result in a complex profile for the COP as a function of the nozzle density and cavity height, revealing a maximum for the COP in the middle range of the nozzle density. As shown in Fig. 16(a) for the inlet diameter ratio of d_i/L = 0.3, the highest COP is found for the range between 30 cm^{-2} and 300 cm^{-2}, and the cavity height effects are negligible between 0.15 mm and 0.6 mm. The region with high COP values becomes narrower as the flow rate increases to 0.6 L/min, as illustrated in Fig. 16(b). The highest COP is now located between the range of 50 cm^{-2} to 100 cm^{-2}.

The profile of the COP surface can be explained based on the hydraulic analysis of the unit cell model. In general, the pressure drop of the unit cell includes several parts: the pressure drop along the inlet/outlet nozzle $\Delta p_{in-nozzle}$ and $\Delta p_{out-nozzle}$, the pressure drop along the cavity channel $\Delta p_{channel}$and the pressure drop generated by the jet cooling Δp_{jet}, and also the pressure loss Δp_{loss} due to the flow expansion and flow contraction. In order to understand the impact of the nozzle density on the pressure drop, a simplified first-order analysis is performed, shown as below:

$$\Delta p_{tot} = \Delta p_{nz-in} + \Delta p_{nz-out} + \Delta p_{ch} + \Delta p_{jet} + \Delta p_{loss} \quad (6)$$

For a constant flow rate, the pressure drop of the cooler Δp_{unit} is very high at thinner cavity thickness H. The reason is that the dominant

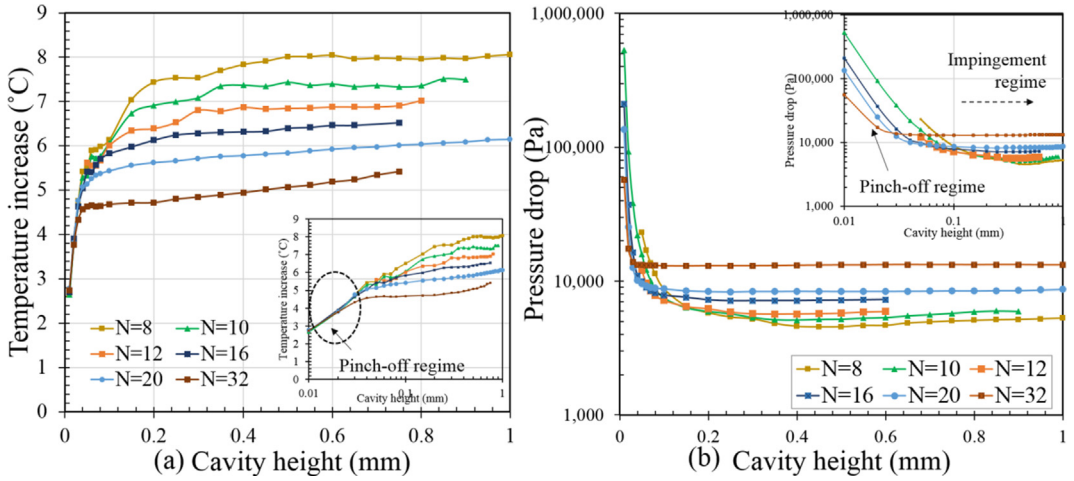

Fig. 15. Unit cell modeling results: (a) temperature increase and (b) pressure drop as function of cavity height between 0.01 mm and 1 mm (d_i/L = 0.3, FL = 600 ml/min).

pressure drop is the pressure drop across the impingement cavity channel Δp_{ch}, which is inversely proportional to the cavity thickness H, shown as below:

$$\Delta p_{ch} \sim \frac{L\dot{V}_n}{H^4} \tag{7}$$

where the $\dot{V}_n$ is the flow rate per nozzle, defined as total flow rate divide total inlet nozzle number $\frac{\dot{V}}{N^2}$. The cavity height H is defined as the hydraulic length for the simplified channel flow model.

On the other hand, for a fixed cavity height H, the pressure drop will be very high for low nozzle density, since the outlet drainage is far from the inlet. As the nozzle density is higher than 100 cm^{-2}, the pressure will also increase due to the scaling down of the nozzle diameter d_i, resulting in a higher pressure drop inside the nozzles Δp_{nozzle}, which can be explained in the following equation (for laminar flow):

$$\Delta p_{in-nozzle} = \frac{8\mu t\dot{V}_n}{\pi (d_i/2)^4} \tag{8}$$

where the nozzle length t is defined as the length of the pipe flow, μ is the dynamic viscosity, $\dot{V}$ is the volumetric flow rate, and d_i is the diameter of the nozzle. The combined effect of the pressure contributions results in a complex behavior as function of the nozzle density.

In summary, for the scaling analysis, a constant nozzle diameter ratio d_i/L is considered, resulting in a constant nozzle velocity regardless of the number N since the total nozzle area remains constant. The pressure drop for high nozzle densities is dominated by the contribution of the pressure drop in the inlet and outlet nozzle. This contribution scales with d_i^{-4} with $\dot{V}_{nozzle}^2$and with the friction factor f. Since:

- o d_i scales with N^{-1}
- o $\dot{V}_{nozzle}$ *scales with* N^{-2}
- o f scales with $Re^{-1} \sim d_i^{-1} \sim N$ (for laminar flow)

Therefore, this contribution scales with N, resulting in a high pressure drop for large nozzle densities.

5.3.2. *Comparison 2: Constant pumping power*

For a constant pumping power consideration, good thermal performance of the cooler is expressed by a low value of the normalized thermal resistance R_{th}. This is equivalent with a high value of the COP, as shown in Eq. (5). The nozzle diameter ratio d_i/L is still kept as 0.3 in this study. The normalized thermal resistance contour is plotted as function of nozzle density and cavity height, for a constant pumping power of 0.1 W/cm^2 and 0.2 W/cm^2, shown in Fig. 17. In general, for a constant cavity height, the thermal resistance decreases as the nozzle density increases. Moreover, it is observed that the lowest thermal resistance is found at the region with higher nozzle density and lower cavity height, which is located at the top left corner of the chart.

Fig. 18 shows the thermal resistance curves as function of the nozzle density and cavity height, for a constant pumping power of 0.2 W/cm^2. It shows that the lowest thermal resistance is in the thin cavity range ("pinch-off") around 10 μm, for different nozzle arrays. For higher

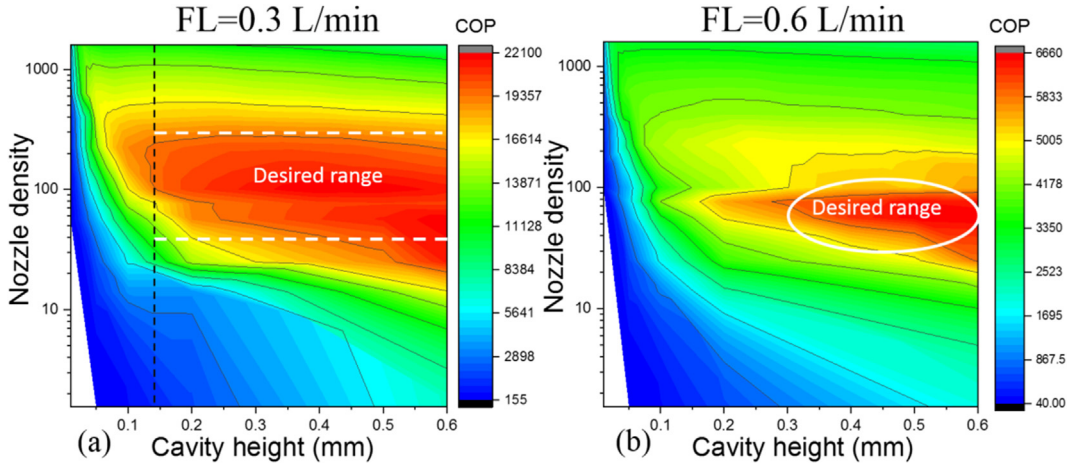

Fig. 16. COP contour as function of the nozzle density and cavity height under different flow rate: (a) FL = 0.3 L/min and (b) FL = 0.6 L/min (d_i/L = 0.3).

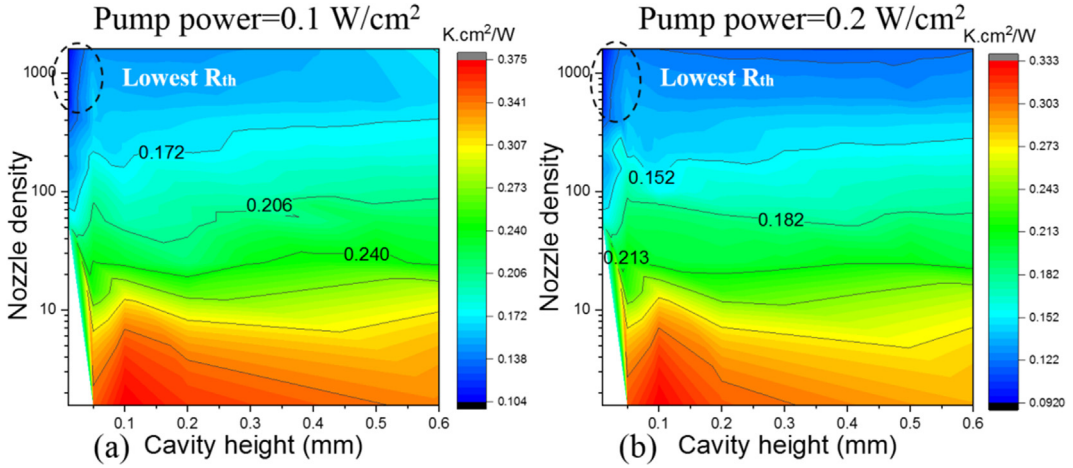

Fig. 17. Characteristic contour of cooler under different required pumping power for a constant $d_i/L = 0.3$: (a) normalized pumping power of 0.1 W/cm^2; (b) normalized pumping power of 0.2 W/cm^2.

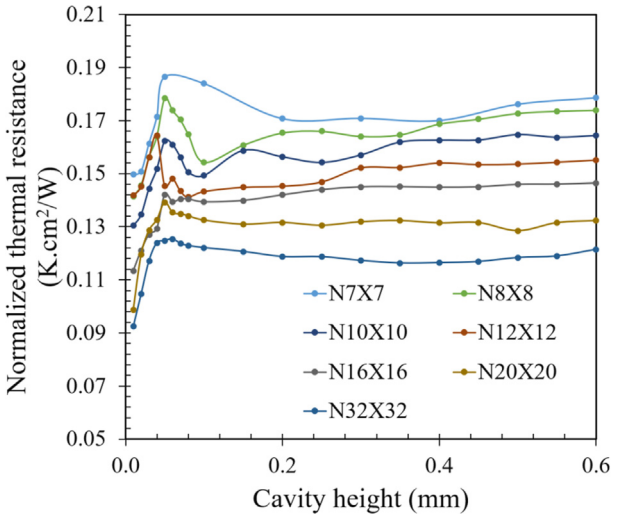

Fig. 18. Thermal resistance curves as function of nozzle density with different inlet diameter ratio, for a constant pumping power ($d_i/L = 0.3$, Wp* = 0.2 W/cm^2).

cavity heights H, beyond 200 μm, defined as the impingement jet regime, the thermal resistance remains stable as a function of the cavity height, with small variations. However, the nozzle scaling trend is different for $d_i/L = 0.1$ and for $d_i/L = 0.3$, as illustrated in Fig. 19. In general, the thermal resistance for the nozzle diameter ratio $d_i/L = 0.3$ is much lower than for $d_i/L = 0.1$, which means that a larger nozzle diameter ratio is better for the thermal cooling performance. Specifically, for constant cavity height at $d_i/L = 0.1$, it shows that the lowest thermal resistance is located in the middle range of the nozzle density around 100 cm^{-2}. For the larger inlet diameter ratio $d_i/L = 0.3$, the thermal performance can be further improved by increasing the nozzle density.

In summary, it is found that a high as possible inlet diameter ratio $d_i/L = 0.3$ is optimal for the cooler design, which is based on the design constraint. As for the impact of nozzle density for a constant pumping power, the optimal design for the nozzle density is around 1,000 cm^{-2}, with optimal cavity height range between 0.01 mm and 0.05 mm, based on the cooler bonding techniques [31].

6. Conclusion

This paper focuses on the nozzle scaling effects of the chip level 3D printed microjet cooler using high resolution additive manufacturing. Firstly, the experimental studies show that a very good thermal performance for 8 × 8 cooler with 1 × 1 mm^2 cooling cells can be achieved as low as 0.13 cm^2-K/W for a flow rate of 1,000 ml/min. Coolers with three nozzle densities have been fabricated and experimentally characterized, including a 3×3, 4×4 and 8×8 inlet nozzle array. A trend of increasing thermal performance for increasing nozzle density has been observed. The comparison between experiments with a thermal test chip and CFD modeling results shows good agreement with maximum difference below 15%. The validated CFD models have been used to extrapolate the experimental data in order the find the optimal cooler geometry and to understand the nozzle scaling effects. To this end, an extensive parameter sensitivity study has been performed with the CFD model by varying the three major design variables: nozzle density: N^2/A, cavity height H and nozzle diameter ratio di/L.

In order to compare the cooling performance for different cooler geometries, two criteria have been considered as the basis for the comparison: (1) constant coolant flow rate and (2) constant pumping power. First, it is found that the nozzle diameter ratio is the dominant parameter with a higher impact than the nozzle density and cavity height. Secondly, it is shown that the best cooler design, expressed as the highest value of the COP, can be achieved in the middle range of the

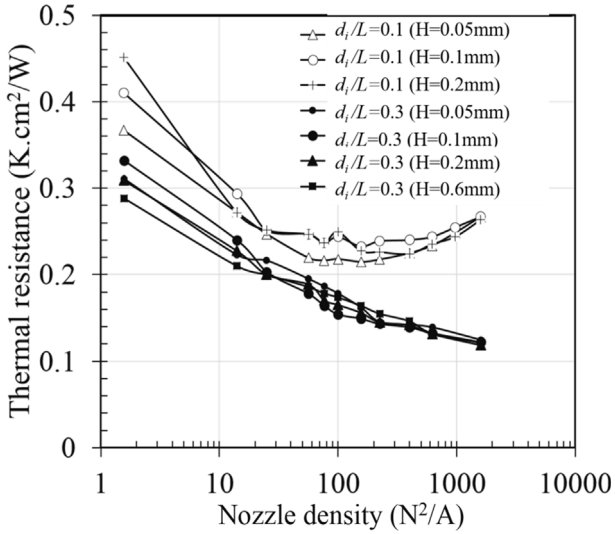

Fig. 19. Thermal resistance curves as function of nozzle density with different inlet diameter ratio, for a constant pumping power (Wp* = 0.2 W/cm^2).

nozzle density between 30 cm^{-2} to 300 cm^{-2} for the constant flow rate consideration. The optimal region for the high COP values becomes narrower as the flow rate increases. For the constant pumping power consideration however, the lowest thermal resistance is found at the values of higher nozzle density and lower cavity height. Moreover, it is shown that the thermal performance can be further improved by increasing the nozzle density, for the larger inlet diameter ratios, whereas a saturation or even reverse trend is found for smaller inlet diameter ratios. This analysis clearly indicates that the optimal design parameters of the impingement cooler strongly depend on basis that is chosen for the comparison of the cooler performance. Comparisons in terms of constant cooler flow rate or constant pumping power will result in different optimal design parameter values.

Declaration of Competing Interest

The authors declare that they have no known competing financial interests or personal relationships that could have appeared to influence the work reported in this paper.

Acknowledgments

This work was performed as part of the imec Industrial Affiliation Program on 3D System Integration and has been strongly supported by the imec partners and the imec Reliability, Electrical testing, Modeling and 3D technology teams.

References

[1] H. Lee, D.D. Agonafer, Y. Won, F. Houshmand, C. Gorle, M. Asheghi, K.E. Goodson, Thermal modeling of extreme heat flux microchannel coolers for GaN-on-SiC semiconductor devices, Journal of Electronic Packaging 138 (2016) 010907.
[2] B.W. Webb, C.-F. Ma, Single-phase liquid jet impingement heat transfer, Advances in Heat Transfer 26 (1995) 105–217.
[3] K. Gould, S.Q. Cai, C. Neft, S. Member, Liquid jet impingement cooling of a silicon carbide power conversion module for vehicle applications, IEEE Trans. Power Electronics 30 (6) (2015) 2975–2984.
[4] R. Skuriat, C.M. Johnson, Thermal performance of baseplate and direct substrate cooled power modules, in: Proc. 4th IET Int. Conf. Power Electron. Mach. Drives, 2008, pp. 548–552.
[5] J. Jorg, S. Taraborrelli, G. Sarriegui, R.W. De Doncker, R. Kneer, W. Rohlfs, Direct single impinging jet cooling of a mosfet power electronic module, IEEE Trans. Power Electronics 33 (5) (2018) 4224–4237.
[6] T. Brunschwiler et al., Direct liquid jet-impingement cooling with micronsized nozzle array and distributed return architecture, in: Proc. IEEE Therm. Thermomechanical Phenom. Electron. Syst., 2006, pp. 196–203.
[7] G. Natarajan, R.J. Bezama, Microjet cooler with distributed returns, Heat Transf. Eng. 28 (8–9) (2010) 779–787.
[8] N. Zuckerman, N. Lior, Jet impingement heat transfer: physics, correlations, and numerical modeling, Adv. Heat Transfer 39 (2006) 565–631.
[9] T. Wei, et al., High-Efficiency Polymer-Based Direct Multi-Jet Impingement Cooling Solution for High-Power Devices, IEEE Trans. Power Electron. 34 (7) (July 2019) 6601–6612.
[10] E.N. Wang, L. Zhang, J.-M. Koo, J.G. Maveety, E.A. Sanchez, K.E. Goodson, T.W. Kenny, Micromachined jets for liquid impingement cooling for VLSI chips, J. Microeletromech. Sys. 13 (5) (October 2004) 833–842.
[11] E.A. Browne, G.J. Michna, M.K. Jensen, Y. Peles, Microjet array single-phase and flow boiling heat transfer with R134a, Int. J. Heat Mass Transf. 53 (23–24) (2010) 5027–5034.
[12] Y. Han, B.L. Lau, G. Tang, X. Zhang, Thermal management of hotspots using diamond heat spreader on Si microcooler for GaN devices, IEEE Trans. Compon. Packag. Manuf. Technol. 5 (12) (2015) 1740–1746.
[13] B.P. Whelan, R. Kempers, A.J. Robinson, A liquid-based system for CPU cooling implementing a jet array impingement waterblock and a tube array remote heat exchanger, Appl. Therm. Eng. 39 (2012) 86–94.
[14] M.R. Overholt, A. McCandless, K.W. Kelly, C.J. Becnel, S. Motakef, "Micro-Jet Arrays for Cooling of Electronic Equipment", in Proc, ASME 3rd International Conference on Microchannels and Minichannels, 2005, pp. 249–252.
[15] T. Acikalin, C. Schroeder, "Direct liquid cooling of bare die packages using a microchannel cold plate," in Proc. IEEE Therm. Thermomechanical Phenom. Electron. Syst., 2014, pp. 673–679.
[16] M.K. Sung, I. Mudawar, Single-phase hybrid micro-channel/micro-jet impingement cooling, Int. J. Heat Mass Transf. 51 (17–18) (2008) 4342–4352.
[17] J. Jorg, S. Taraborrelli, et al., "Hot spot removal in power electronics by means of direct liquid jet cooling," in Proc. IEEE Therm. Thermomechanical Phenom. Electron. Syst., 2017, pp. 471–481.
[18] A. J. Robinson, W. Tan, R. Kempers, et al., "A new hybrid heat sink with impinging micro-jet arrays and microchannels fabricated using high volume additive manufacturing," in Proc. IEEE Annu. IEEE Semicond. Therm. Meas. Manag. Symp., 2017, pp. 179–186.
[19] T. Wei et al., Experimental Characterization of a Chip Level 3D Printed Microjet Liquid Impingement Cooler for High Performance Systems, in: IEEE Transactions on Components, Packaging and Manufacturing Technology. doi: 10.1109/TCPMT.2019.2905610.
[20] D.J. Womac, S. Ramadhyani, F.P. Incropera, Correlating Equations for Impingement Cooling of Small Heat Sources with Single Circular Liquid Jets, J. Heat Transfer 115 (1) (1993) 106–115.
[21] S.V. Garimella, R.A. Rice, Confined and Submerged Liquid Jet Impingement Heat Transfer, J. Heat Transfer 117 (4) (1995) 871–877, https://doi.org/10.1115/1.2836304.
[22] S.V. Garimella, V.P. Schroeder, Local heat transfer distributions in confined multiple air jet impingement, J. Electron. Packag. 123 (3) (2001) 165–172.
[23] L.B.Y. Aldabbagh, I. Sezai, Numerical simulation of threedimensional laminar multiple impinging square jets, Int. J. Heat Fluid Flow 23 (4) (2002) 509–518, https://doi.org/10.1016/S0142-727X(02)00141-8.
[24] A. Husain, et al., Thermal performance analysis and optimization of microjet cooling of high-power light-emitting diodes, J. Thermophys Heat Transfer 27 (2) (April 2013) 235–245, https://doi.org/10.2514/1.T3931.
[25] G.M. Chrysler, R.C. Chu, R.E. Simons, Jet impingement boiling of a dielectric coolant in narrow gaps, in: Proceedings of 1994 4th Intersociety Conference on Thermal Phenomena in Electronic Systems (I-THERM), Washington, DC, USA, 1994, pp. 1–8.
[26] Bryon Moyer, Spray-On Cooling, EE journal, October, 2018.
[27] H. Oprins, V. Cherman, T. Webers, et al., Characterization and benchmarking of the low intertier thermal resistance of three-dimensional hybrid Cu/dielectric wafer-to-wafer bonding. ASME. J. Electron. Packag. 2017;139(1):011008-011008-9.
[28] J. Pfitzner, Poiseuille and his law, Anaesthesia. 31 (2) (1976) (published Mar 1976). pp. 273–5.
[29] P.A. de Oliveira, J.R. Barbosa, Novel two-phase jet impingement heat sink for active cooling of electronic devices, Appl. Therm. Eng. 112 (5) (2017) 952–964.
[30] S. K. Waye, S. Narumanchi, M, et al., Advanced liquid cooling for a traction drive inverter using jet impingement and microfinned enhanced surfaces, in: Fourteenth Intersociety Conference on Thermal and Thermomechanical Phenomena in Electronic Systems (ITherm), Orlando, FL, 2014, pp. 1064-1073.
[31] Daniel Bae, Raphael Mandel, Michael Ohadi, Effect of bonding structure and heater design on performance enhancement of feeds embedded Manifold-Microchannel cooling, InterPACK (2017) 74158.
[32] T.W. Wei, H. Oprins, V. Cherman, E. Beyne, M. Baelmans, Conjugate heat transfer and fluid flow modeling for liquid microjet impingement cooling with alternating feeding and draining channels, Fluids 4 (3) (2019) 145.
[33] Mark E. Steinke, Satish G. Kandlikar, Single-phase liquid heat transfer in plain and enhanced microchannels, in: ASME 4th International Conference on Nanochannels, Microchannels, and Minichannels, American Society of Mechanical Engineers Digital Collection, 2006, pp. 943–951.